Heliyon 10 (2024) e30008

Contents lists available at ScienceDirect

Heliyon

journal homepage: www.cell.com/heliyon

Research article

Aberrant concordance among dynamics of spontaneous brain activity in patients with migraine without aura: A multivariate pattern analysis study

Yilei Chen [a], Jun Xu [b], Jiazhen Wu [c], Hui Chen [a], Yingjie Kang [a], Yuchan Yang [a], Zhigang Gong [a], Yanwen Huang [a], Hui Wang [a], Bo Wang [d], Songhua Zhan [a], Wenli Tan [a,*,1]

[a] *Department of Radiology, Shuguang Hospital Affiliated to Shanghai University of Traditional Chinese Medicine, Shanghai, China*
[b] *Pharmacy Department, Shanghai Municipal Hospital of Traditional Chinese Medicine, Shanghai University of Traditional Chinese Medicine, Shanghai, China*
[c] *Department of Radiology, Shanghai Municipal Hospital of Traditional Chinese Medicine, Shanghai University of Traditional Chinese Medicine, Shanghai, China*
[d] *Department of Acupuncture and Moxibustion, Shuguang Hospital Affiliated to Shanghai University of Traditional Chinese Medicine, Shanghai, China*

ARTICLE INFO

Keywords:
Migraine
Spontaneous brain activity
Concordance
Multi-voxel pattern analysis

ABSTRACT

Background: Alterations in the static and dynamic characteristics of spontaneous brain activity have been extensively studied to investigate functional brain changes in migraine without aura (MwoA). However, alterations in concordance among the dynamics of spontaneous brain activity in MwoA remain largely unknown. This study aimed to determine the possibilities of diagnosis based on the concordance indices.

Methods: Resting-state functional MRI scans were performed on 32 patients with MwoA and 33 matched healthy controls (HCs) in the first cohort, as well as 36 patients with MwoA and 32 HCs in the validation cohort. The dynamic indices including fractional amplitude of low-frequency fluctuation, regional homogeneity, voxel-mirrored homotopic connectivity, degree centrality and global signal connectivity were analyzed. We calculated the concordance of grey matter volume-wise (across voxels) and voxel-wise (across time windows) to quantify the degree of integration among different functional levels represented by these dynamic indices. Subsequently, the voxel-wise concordance alterations were analyzed as features for multi-voxel pattern analysis (MVPA) utilizing the support vector machine.

Results: Compared with that of HCs, patients with MwoA had lower whole-grey matter volume-wise concordance, and the mean value of volume-wise concordance was negatively correlated with the frequency of migraine attacks. The MVPA results revealed that the most discriminative brain regions were the right thalamus, right cerebellar Crus II, left insula, left precentral gyrus, right cuneus, and left inferior occipital gyrus.

Conclusions: Concordance alterations in the dynamics of spontaneous brain activity in brain regions could be an important feature in the identification of patients with MwoA.

* Corresponding author.
E-mail address: tanying2245@163.com (W. Tan).
[1] Present address: No. 528, Zhangheng Road, Pudong New Area, Shanghai, China.

https://doi.org/10.1016/j.heliyon.2024.e30008
Received 5 October 2023; Received in revised form 8 April 2024; Accepted 18 April 2024
Available online 30 April 2024

1. Introduction

Migraine is a widespread headache condition distinguished by repetitive occurrences and throbbing head pain, which may arise due to various physical or environmental factors [1] and is the second most frequent source of disability [2]. The symptoms include moderate to severe headache; nausea; vomiting; and sensitization of the visual, auditory, and olfactory systems [3]. Due to its widespread occurrence, economic impact, and impact on daily functioning, migraine has emerged as a significant public health concern. Migraine without aura (MwoA) represents the prevailing form of migraine headaches encountered [4]. Current theories on migraine pathophysiology are mainly concerned with the activation and sensitization of the trigeminovascular system [5], whereas the pathogenesis of migraine is intricate and varied. This complexity of migraine also leads to the poor outcomes and recurrence.

As migraine is primarily a functional brain disorder, functional MRI (fMRI) techniques can provide a pathway for investigating its underlying mechanisms [6,7]. Numerous studies have indicated that the onset of migraines is linked with hyperexcitability in the hypothalamus and early reorganisation of ascending pain and central trigeminovascular pathways, including the insula, brainstem, limbic system, hypothalamus, thalamus, and certain functional networks. The methodology used in these studies included static and dynamic functional connectivity (FC), effective connectivity (EC), graph theory analysis, and local brain activity [8–13]. However, the reproducibility of the results of these studies is poor, and a direct comparison of these fMRI indices is lacking.

In recent years, leveraging advancements in machine learning, researchers have introduced the multivariate pattern analysis (MVPA) method. This data-driven approach utilizes pattern recognition principles to decode relationships between neural signals and external stimuli or cognitive states by employing multivariate models [14], which have been frequently utilized to analyze spatial pattern data for fMRI categorization and prediction [15]. MVPA offers several advantages over conventional univariate analysis. Unlike the voxel-centric approach of univariate methods, MVPA analyzes patterns across multiple voxels, revealing subtle variations in neural representations. This holistic analysis mitigates limitations imposed by low signal-to-noise ratios and stringent multiple comparison corrections. Additionally, MVPA demonstrates greater resilience to sample size constraints, even enabling decoding of cognitive states from single trials in some cases. Furthermore, it integrates signals from spatially distinct brain regions, elucidating the functional interplay critical for complex cognitive processes [16,17]. MVPA has shown promise in identifying and predicting individual patients with Internet gaming disorder [18], depressive disorder [19], essential tremor [20], dispositional worry [21], and patients with panic disorder [22].

An increasing number of studies has taken advantage of the temporal changes in rs-fMRI indices to investigate the mechanism of diseases. These indices serve as indicators of spontaneous brain activity include the fractional amplitude of low-frequency fluctuation (fALFF), regional homogeneity (ReHo), voxel-mirrored homotopic connectivity (VMHC), Degree Centrality (DC), and Global Signal Connectivity (GSC). Yan et al. conducted an in-depth analysis of the spatial and temporal connections between various resting-state brain activity metrics, revealing a high degree of covariance among these metrics. Subsequently, they determined the voxel-wise within-subject concordance by calculating Kendall's W for brain activity metrics across time windows at each voxel. Similarly, volume-wise concordance was obtained by calculating Kendall's W for brain activity metrics across all voxels for each time window, analyses of concordance, defined by the co-occurrence of temporal and spatial dynamics across multiple indices of brain activity, revealed significant inter-individual differences that were stable over time. Furthermore, a notable correlation emerged between concordance and age, suggesting a potential functional link between this co-activation and cognitive processes [23]. Furthermore, an increasing number of research have demonstrated that concordance shows stable individual differences in Parkinson's disease [24], Alzheimer's disease [25], major depressive disorder [26,27], and schizophrenia [28], suggesting that this approach might give a fresh insight into the underlying mechanisms of migraine. However, to our knowledge, limited studies using MVPA have provided the classification performance of the concordance of alterations on rs-fMRI in patients with MwoA.

Hence, in the current study, we first utilized MVPA to identify brain regions exhibiting differential concordance profiles within spontaneous brain dynamics between patients with MwoA and healthy controls (HCs). Subsequently, the applicability of these MwoA-discriminative brain regions was assessed using an independent dataset. We hypothesized that the concordance of spontaneous dynamic changes in fALFF, ReHo, VMHC, DC, and GSC would be altered and could identify individuals in patients with MwoA.

2. Materials and methods

2.1. Participants

This study included two cohorts of individuals with MwoA and HCs. The first cohort, which comprised 35 patients with MwoA and 34 age- and gender-matched HCs, was recruited between 8 April 2018 and 6 October 2019. To confirm the machine learning classification findings acquired from the first cohort, the second cohort was recruited from 23 February 2021 to 24 February 2022 and included 38 MwoA patients and 32 age- and sex-matched HCs. Patients with MwoA were recruited from among the outpatients in the acupuncture department of Shuguang Hospital affiliated with the Shanghai University of Traditional Chinese Medicine. MwoA was diagnosed according to the ICHD-III criteria of the International Classification of Headache Disorders, 3rd Edition [29]. The inclusion criteria were as follows: 1) age 18–65 years and right-handed; 2) experience of a unilateral and/or pulsating headache; 3) occurrence of a headache attack at least once a month for the past 3 months; 4) did not undergo physical therapy or used preventive headache medication in the past month; and 5) did not ingest psychotropic or vasoactive medications in the past 3 months. The exclusion criteria were as follows: 1) existence of other comorbid chronic pain conditions, 2) a history of brain trauma or tumour, 3) suffering from any other neurological or psychiatric disorders, 4) a history of drug or alcohol abuse, and 5) any fMRI contraindications. The Ethics

Committee of Shuguang Hospital, which is affiliated with Shanghai University of Traditional Chinese Medicine, approved this trial, which is documented at www.chictr.org.cn (ChiCTR1900023105). Written informed consent was obtained from all participants.

2.2. Clinical assessment

Rating scores, including the visual analogue scale (VAS) (0−10) for pain intensity, frequency of migraine attacks (days/month), Self-Rating Anxiety Scale (SAS), Self-Rating Depression Scale (SDS), and Migraine-Specific Quality of Life Questionnaire scores (MSQ), were acquired for each patient with MwoA [12].

2.3. MRI data acquisition

Both cohorts underwent magnetic resonance imaging (MRI) scans using a 3T MRI scanner (United Imaging Medical Systems, Shanghai, China) equipped with a 12-channel flexible head coil. The first cohort was scanned on the uMR780 scanner, while the second cohort utilized the uMR790 scanner. The sequences and parameters were identical in both the first and second cohorts. The echo-planar imaging sequence was employed to record the remaining fMRI images using the following parameters: repetition time (TR) = 2 s, echo time (TE) = 30 ms, flip angle = 90°, matrix size = 64 × 64, 33 slices, slice thickness = 4 mm, superior-inferior field-of-view = 256 mm, and 240 volumes. A 3D-T1-weighted fast spoiled gradient echo sequence was used to obtain structural images, and the parameters were as follows: TR = 2050 ms, TE = 3.8 ms, flip angle = 9°, field of view = 220 × 220 mm^2, matrix size = 256 × 256, 160 slices, and slice thickness = 1.0 mm. A cushion was inserted in the coil to decrease movement and stabilize the head. The participants were told to shut their eyes and relax, but not sleep, while not thinking about anything.

2.4. fMRI data preprocessing

Fig. 1 shows the flow diagram of the analysis technique used in the current study. The Data Processing Assistant for Resting-State fMRI software (http://rfmri.org/DPABI) on the MATLAB 2013b (https://www.mathworks.com/) platform was used to preprocess the functional resting-state data. The preprocessing steps for each individual's functional resting-state were as follows. Images from the initial ten time points were eliminated, while the remaining 230 time points were utilized for data analysis. To correct head motion, the timing and realignment of the slices were carried out, ensuring that no more than 2.0 mm or 2.0° were observed in the translation or rotation motion of any given data. The co-registered functional images were subjected to spatial normalization in the Montreal Neurological Institute's space and then resampled into 3-mm cubic voxels. To mitigate the impact of low-frequency drifts, we performed a nuisance covariate regression that included the white matter signal, cerebrospinal fluid signal, and 24 head-motion parameters.

2.5. Calculation of rs-fMRI indices of dynamics

Five rs-fMRI indices were used in the concordance analysis, which were fALFF, ReHo, VMHC, DC, and GSC.

2.5.1. fALFF

ALFF was calculated by taking the mean amplitude of a time series in a specific frequency range (0.01–0.1 Hz) following Fourier

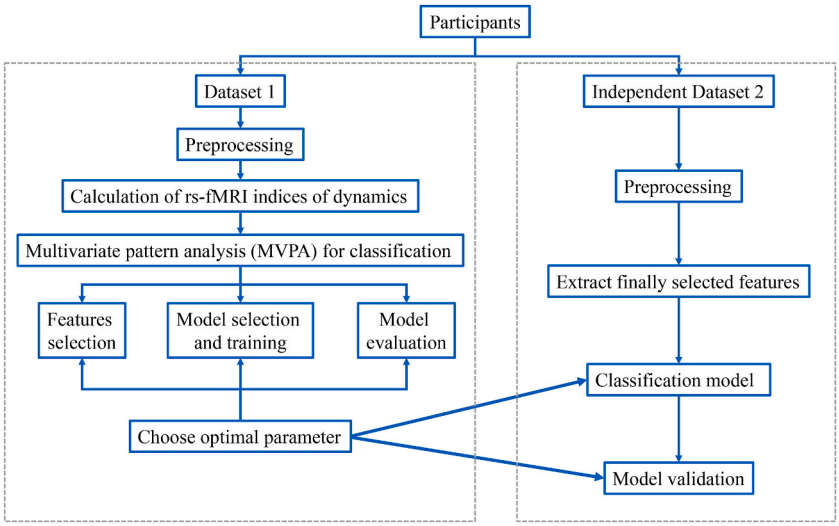

Fig. 1. Flowchart of this study. Abbreviations: ROI, region of interest.

transformation [30], while the fALFF value was calculated as the ratio of low-frequency power spectrum (0.01–0.1 Hz) to the total power spectrum within the specified frequency range [31]. Due to the robust correlation observed between ALFF and fALFF, we selected fALFF for the concordance analysis due to its heightened sensitivity and specificity in identifying spontaneous brain activity [32].

2.5.2. ReHo

ReHo was employed to quantify the synchronization of neural activity within a local brain area over a given period, defined as Kendall's W coefficient of concordance between the time series of a particular voxel and those of its immediate neighbors (26 voxels) [33].

2.5.3. VMHC

The BOLD signal time-series Pearson correlation coefficient between particular voxels in the symmetrical areas of the left and right hemispheres was employed to determine the VMHC [34].

2.5.4. DC

DC is defined by the number of edges connected to a node in binary graphs or the total weight of the edges connected to a node in weighted graphs. In functional connectivity studies of the brain, a common method is to calculate the Pearson correlation coefficients between BOLD time series of various brain regions (or voxels) to obtain a grey matter functional connectivity matrix. The DC represents the cumulative count of connections exceeding a correlation coefficient of 0.25 throughout all its associated edges for each voxel [35].

2.5.5. GSC

The mean time series of all voxels within the group-level mask was first calculated by employing the GSC as the global signal. Subsequently, the Pearson correlation coefficient between the time series of each voxel within the group-level mask and the global signal was determined. The GSCorr value used in the subsequent calculations was the standardised score obtained after Fisher-Z transformation [36].

After these five types of rs-fMRI measures were completed, the Temporal Dynamic Analysis (TDA) toolkit, based on DPABI V6.0, was employed to examine the dynamics of these rs-fMRI indices [37]. A Hamming window with a window size of 50 TR and window stride of 1 TR was applied to segment the functional images of each participant, and a series of BOLD signal windows were obtained. Subsequently, these rs-fMRI metrics for each window were computed. To quantitatively characterise the temporal dynamic features of each index, the standard deviation (SD) of each index was calculated for each voxel over time in the whole brain. The SD maps were subjected to *Z*-score normalization using a group mask for statistical analysis. Finally, the normalized SD maps of each dynamic rs-fMRI index were smoothed using a Gaussian kernel with a $4 \times 4 \times 4$ mm^3 full-width at half maximum (FWHM) in order to improve the signal-to-noise ratio.

2.6. Volume-wise and voxel-wise concordance

Kendall's W method was used to assess volume- and voxel-wise concordance. This non-parametric statistic does not make any assumptions regarding the distribution and remains unaffected by the magnitude of disparities among the five dynamic rs-fMRI indices (including ALFF, ReHo, DC, VMHC, and GSC) [23]. Two types of concordance indices were calculated: 1) Volume-wise concordance index: first, for each window, the Kendall W value was computed for the five indices spanning across voxels. The average value of the volume-wise concordance for each participant was then calculated for all time windows and used as the basis for the results. 2) Voxel-wise concordance index: the voxel-wise concordance between the time windows for each participant was calculated. To facilitate subsequent analyses, a Gaussian kernel with an FWHM of 4 mm was used to smooth the voxel-wise concordance maps [38].

2.7. Multivoxel pattern analysis

We utilized the Pattern Recognition for Neuroimaging Toolbox (PRoNTo v2.0; http://www.mlnl.cs.ucl.ac.uk/pronto/) within the MATLAB environment to identify brain regions exhibiting the greatest discriminatory power in differentiating patients with MwoA from HCs. For a detailed description of the MVPA technique, refer to Schrouff et al. [39]. Briefly, the main steps included the following. (a) Data and design: the voxel-wise concordance maps of patients with MwoA and HCs was loaded. (b) Prepare the future set: 3D images derived from voxel-wise concordance maps were transformed into feature vectors. This process involved vectorizing each image, where each element in the resulting vector corresponded to the intensity of its corresponding voxel in the original 3D image. Thus, voxel-wise concordance values were considered features, and the average DARTEL GM mask was utilized to exclude features of no interest. (c) Specify and run the model: the participants were split into training and testing sets. Given the limited number of participants in this study, leave-one-subject-out-cross-validation (LOSOCV) was adopted to assess the generalisability of the classification model. Specifically, one sample (based on a voxel-wise concordance map) was extracted from the dataset as the testing data, whereas the remaining dataset was used to train the classification model. This process was repeated for each participant to obtain a relatively unbiased estimate of the generalisation rates. The PRoNTo software automatically handled the aforementioned process and generated the PRoNTo (PRT) maps. (d) Compute weights: the weights of various brain regions were calculated using the Anatomical Automatic Labelling template. (e) Display results: to assess the classification models' performance following PRT diagram loading,

sensitivity, specificity, accuracy, and receiver operating characteristic curves were generated. Each classification was iterated 1000 times, and corrected p-values were employed to determine the statistical significance. (f) Display weights: following the weight calculation, the PRT diagram was loaded, and the weights of each region of interest, according to the atlas definition, were displayed. The contributions of the regions to the classification models were sorted and listed in descending order. We computed the vector weights and listed the top 10 % [40] of regions with a cluster size of >100 voxels to investigate their classification abilities [41]. In this study, the validation of machine learning results derived from the first cohort was conducted using the second cohort. We first applied MVPA to classify patients in the first cohort, identifying the top 10 % weighted regions, which were then used as features in an SVM analysis on patients in the second cohort to assess the robustness of these regions.

2.8. Statistical analysis

SPSS software (version 25.0; SPSS Inc., Chicago, IL, USA) was used to assess the demographic attributes of the MwoA and HCs groups. A two-sample *t*-test was employed to examine the disparity in age between the two cohorts, while the $\chi 2$ test was utilized to assess the disparity in sex between the two groups. Intergroup differences in volume-wise concordance were analyzed using a two-sample *t*-test, with age, sex, and head motion as covariates. Statistical significance was set at P value < 0.05. Partial correlations were examined to investigate the association between the volumetric concordance of patients with MwoA exhibiting notable inter-group disparities and clinical parameters (e.g., disease duration, migraine attack frequency, VAS, SAS, SDS, and MSQ scores) while adjusting for covariates like age, gender, and head motion. Bonferroni correction was applied for multiple comparisons, with the significance level set at $p < 0.05/6$.

3. Results

3.1. Demographics and clinical characteristics

Six subjects were removed after head motion control (three patients with MwoA and one HC in cohort 1 and two patients with MwoA in cohort 2). Ultimately, this study enrolled 32 participants with MwoA and 33 HCs in cohort 1, as well as 36 participants with MwoA and 32 HCs in cohort 2. Table 1 displays the demographic and clinical profiles of the participants. No statistically significant differences were observed between the two patient groups concerning age, gender, educational level, height, and weight.

3.2. Volume-wise concordance alterations in patients with MwoA

Patients with MwoA exhibited a significantly decreased mean value of volume-wise concordance compared to that of HCs ($t = 9.949$, $P < 0.001$) (Fig. 2A). Additionally, we observed a significant negative association between the mean value of volume-wise concordance and frequency of migraine attack ($r = -0.472$, $P = 0.006$) (Fig. 2B). There were no statistically significant correlations found among the other clinical variables, including VAS score, SAS score, SDS score, MSQ score, and disease duration.

3.3. Classification performances for the voxel-wise concordance alterations

In the first cohort, voxel-wise concordance exhibited comparable spatial distributions in both HCs and patients with MwoAs, characterised by extensive grey matter regions that displayed significant temporal concordance (Fig. 3). The MVPA classifier might be employed to differentiate between patients with MwoA and HCs, as evidenced by its 0.83 AUC, 81.54 % accuracy (permutation $P < 0.001$), 90.63 % sensitivity, and 72.73 % specificity, which were determined through voxel-wise concordance spatial distributions (Fig. 4A–C). The most informative regions for classifying patients with MwoA and HCs were the right thalamus (Thalamus_R), right

Table 1
The demographic and clinical characteristics of all participants.

Characteristics	Cohort 1		*P*	Cohort 2		*P*
	MWoA (n = 32)	HCs (n = 33)		MWoA (n = 36)	HCs (n = 32)	
Age (yr)	37.44 ± 10.17	33.26 ± 5.76	0.337	34.57 ± 11.48	31.23 ± 10.88	0.478
Gender (male/female)	5/27	7/26	0.751	9/27	7/25	0.783
Education (years)	15.49 ± 3.03	15.76 ± 1.76	0.341	15.36 ± 2.67	16.11 ± 2.84	0.324
Height (cm)	162.16 ± 6.21	165.12 ± 8.11	0.432	163.46 ± 5.97	164.87 ± 9.12	0.612
Weight (kg)	52.14 ± 6.44	53.89 ± 7.79	0.315	51.23 ± 6.22	54.15 ± 6.32	0.267
Disease duration (years)	15.45 ± 11.48	NA	–	16.05 ± 11.28	NA	–
Frequency of migraine attack (days/month)	4.25 ± 1.95	NA	–	4.98 ± 1.24	NA	–
VAS	6.65 ± 1.26	NA	–	7.14 ± 1.84	NA	–
SAS	45.23 ± 7.14	NA	–	47.21 ± 8.08	NA	–
SDS	49.35 ± 8.39	NA	–	50.31 ± 8.67	NA	–
MSQ scores	62.11 ± 17.55	NA	–	62.35 ± 18.66	NA	–

Abbreviations: MWoA, migraine without aura; HCs, healthy controls; VAS, Visual Analogue Scale; SAS, Self-Rating Anxiety Scale; SDS, Self-Rating Depression Scale; MSQ, Migraine-Specific Quality of Life Questionnaire.

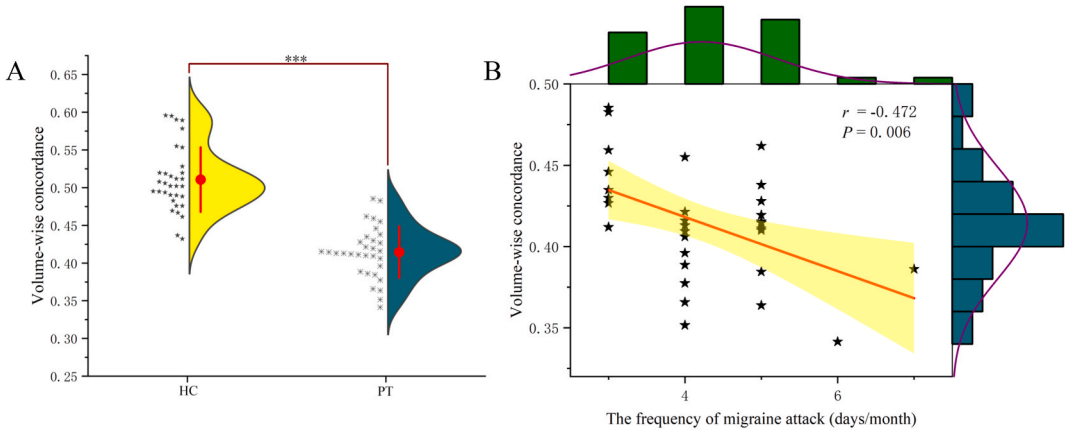

Fig. 2. Volume-wise concordance changes in patients with MwoA. (A) Comparison of mean volume-wise concordance indices between patients with MwoA and HCs. (B) Correlation between volume-wise concordance and frequency of migraine attack in patients with MwoA.

cerebellar Crus II, left insula (Insula_L), left precentral gyrus (Precentral_L), right cuneus (Cuneus_R), and left inferior occipital gyrus (Occipital_Inf_L) (Table 2). The classification models trained on voxel-wise concordance in the first cohort were applied immediately to the second cohort, which reported 0.77 AUC of the classifier, 76.47 % accuracy (permutation $P < 0.001$), 83.33 % sensitivity, and 68.75 % specificity (Fig. S1), demonstrating strong generalisability in an independent cohort.

4. Discussion

In this study, we investigated the aberrant concordance of intrinsic brain activity in patients with MwoA using a dynamic analysis of rs-fMRI data. Specifically, the major findings were as follows. (i) Patients with MwoA showed a decrease in volume-wise concordance compared to that of HCs, which was negatively correlated with migraine attack frequency. This indicated a significant decline in functional integration ability in patients with MwoA. (ii) The image-based MVPA technique using voxel-wise concordance maps can differentiate between patients with MwoA and HCs in another independent patient cohort. These results indicate that spatial and temporal decoupling of multiple rs fMRI indicators could contribute to the understanding of the underlying neuropathological mechanisms in MwoA.

Previous rs-fMRI studies using ALFF, fALFF, and ReHo as features have shown that patients with MwoA exhibit widespread spontaneous brain activity alterations in multiple brain regions compared to those of HCs [42–49]. These brain regions include the middle temporal gyrus, frontal cortex, and cerebellum. However, most studies on migraine have concentrated on utilizing a single rs-fMRI measure, and the abnormal brain regions identified in these studies were significantly different. Multiple factors have contributed to these inconsistent results. Heterogeneity may be introduced objectively using different analytical techniques with different theoretical assumptions. These analyses, with different sensitivities and specificities, made it difficult to reach a consensus on the brain regions affected by migraines. Various rs-fMRI indicators reveal distinct facets of spontaneous brain activity. The consistency among these metrics demonstrates the degree of integration at various functional levels [23]. The concordance of rs-fMRI metrics provides a quantitative method to describe the consistency among a set of basic indicators, which might help characterise spontaneous neural activity from multiple complementary perspectives. Our results showed that patients with MwoAs had significantly lower mean volume-wise concordance than that of HCs, indicating the presence of decreased coherence and synchronization in these patients. The results of this study are in agreement with previous research indicating a decreased synchronization of spontaneous neural activity between the default mode, salience, and sensory-motor networks in MwoA [50]. Additionally, we observed a negative correlation between the mean value of volume-wise concordance and the frequency of migraine attacks. Therefore, a decreased concordance may

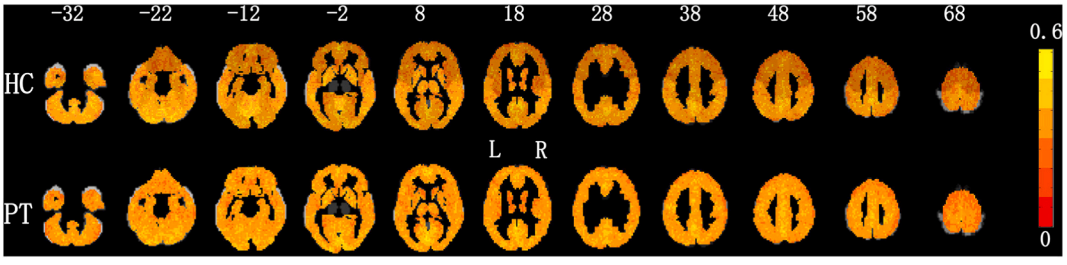

Fig. 3. Spatial distribution maps of voxel-wise concordance. The voxel-wise concordance maps are averaged across subjects in patients with MwoA and HCs, respectively. Abbreviations: HC, healthy controls; PT, Patient; L, left; R, right.

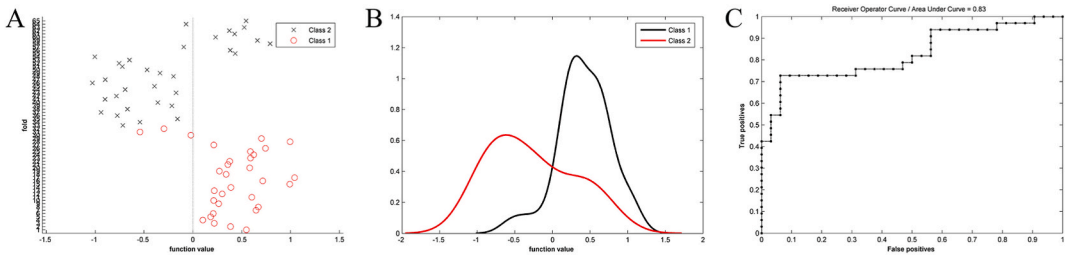

Fig. 4. Discriminant results from the classification based on spatial distributions of the voxel-wise concordance. (A) Scatterplots show the discrimination between the two groups. (B) Histograms of the function values show the discrimination between the two groups. (C) ROC curve shows the performance of classifier.

Table 2
Represent 10 % of the total weights for the classification between patients with MwoA with and HCs according to normalized weights per region.

Brain regions	Peak MNI (mm)	Voxels	% NW
	X Y Z		
Thalamus_R	12.0 −18.0 −6.0	315	2.286
Right cerebellar Crus II	30.0 −75.0 −39.0	235	2.132
Insula_L	−36.0 9.0 3.0	297	1.846
Precentral_L	−39.0 −3.0 51.0	200	1.775
Cuneus_R	12.0 −78.0 27.0	263	1.565
Occipital_Inf_L	−39.0 −78.0 −6.0	216	1.264

Abbreviations: Thalamus_R, right thalamus; Insula_L, left insula; Precentral_L, left precentral gyrus; Cuneus_R, right cuneus; Occipital_Inf_L, left inferior occipital gyrus; % NW: Percentage of the total normalized weights that each anatomical region explains.

be associated with increased disease severity. The observed negative correlation between the mean value of volume-wise concordance and the frequency of migraine attacks supported the theory that recurrent migraines contributed to cumulative neurological damage [51,52]. It was worth noting that the volume-wise concordance method allowed for a global description of multiple functional indicators, but lacked regional specificity, which might limit its ability to identify functional abnormalities in specific brain regions.

In this study, we investigated the differences in voxel-wise concordance between patients with MwoA and HCs and developed a machine learning-based automatic classification method to improve the diagnostic efficiency of MwoA. Using fMRI and an automated data analysis pipeline, we compared the neuronal activity patterns of patients with MwoA and HCs in various brain regions at rest and found significant differences in some important areas, although the voxel-wise concordance was similar. Based on these differences, we trained an MVPA classifier that could effectively distinguish between patients with MwoA and HCs and demonstrated good generalisation performance in an independent test group. These results offer fresh perspectives on the neurobiological mechanisms of MwoA, aid in early diagnosis, and provide treatment strategies for this disease. Specifically, this study revealed differences in neuronal activity patterns in certain brain regions, including the thalamus, cerebellar Crus II, insula, precentral gyrus, cuneus, and inferior occipital gyrus. These brain regions play crucial roles in the neurobiological mechanisms of MwoA and have been confirmed in previous studies. For instance, changes in thalamic function during migraines can be understood by considering the essential role of the thalamus as a key sensorial hub [53]. The insula may serve as a crucial node in the pathophysiology of migraines and play a role in pain processing [54]. The cuneus and the inferior occipital gyrus are parts of the visual network. Heightened reactivity of the advanced visual processing network to painful trigeminal nerve stimulation in migraines has been previously reported [55]. The cerebellar Crus II may be the hub of the cerebellar system [56–58]; nevertheless, there is limited literature on the association between cerebellar function and MwoA. This study highlights the significant involvement of cerebellar Crus II in the central processing of pain perception in MwoA, as evidenced by local brain activity analysis. Furthermore, the MVPA classifier used in this study achieved significant results, with an AUC of 0.83 and an accuracy of 81.54 % for the automatic classification of MwoA patients and HCs. Compared with traditional methods, the MVPA classifier leveraged information from multiple brain regions and used data-driven feature selection algorithms to identify the most discriminative brain regions. It also allowed for automatic updating of feature selection and classifier settings based on changes in data to achieve robustness. Finally, the classifier's generalisation performance was validated on an independent test group, showing that it maintained good performance with an AUC of 0.77 and an accuracy of 76.47 %. This demonstrated the potential clinical applications and robust generalisation capabilities of the classifier. Our findings contributed to the growing body of literature and supported the use of imaging techniques, such as fMRI to better understand the neurobiological mechanisms of migraine. Moreover, these results added to the evidence that support the use of machine learning algorithms for the classification of neurological disorders based on imaging data [22,47,59–61]. With the increasing availability of large-scale datasets, machine learning-based methods have become important tools for the diagnosis and treatment of neurological disorders. In summary, this study opened new perspectives on the neurobiological mechanisms of MwoAs and demonstrated the potential of machine learning-based techniques for improved diagnostic accuracy. Further research is warranted to confirm these findings and explore their clinical applications.

5. Limitation

There were several limitations to this study. Firstly, the size of the sample was limited, restricting the generalisability of our conclusions. Hence, a study employing the identical approach with an expanded sample size is essential to verify the current outcomes. Secondly, using MVPA, we identified the brain regions that are most discriminative. However, future studies should consider the valuable information that may be found in the excluded brain regions. Thirdly, this study had a cross-sectional design and thus could not establish causal relationships. A longitudinal investigation of volumetric changes in patients with MwoA will provide evidence of the progression of disease-related brain changes and identify possible targets for preventive treatment strategies; future studies could include this missing aspect. Finally, we selected only five commonly used rs-fMRI indices for concordance analysis without performing seed-based functional connectivity or independent component analysis. Future research endeavors should prioritize the inclusion of additional fMRI indices for a comprehensive analysis.

6. Conclusion

This study utilized a dynamic analysis approach to investigate the variability and concordance of rs-fMRI indices in patients with MwoA. The spatial and temporal coupling relationships among these indicators were disrupted. We found that MVPA, based on voxel-wise concordance alterations, could stably detect the abnormal functional changes in patients with MwoA at the individual level. These findings offer new perspectives on the neuropathological mechanisms underlying MwoA.

Ethical statement

The Ethics Committee of Shuguang Hospital, which is affiliated with Shanghai University of Traditional Chinese Medicine (approval number: 2018-600-29-01), approved this trial, which is documented at www.chictr.org.cn (ChiCTR1900023105).

Funding

This work was supported by funding from Shanghai Health Care Commission Project (No. 202040194) and Science and Technology Commission of Shanghai Municipality (No. 22Y11910600).

Data availability statement

Data can be made available upon request.

CRediT authorship contribution statement

Yilei Chen: Writing – original draft. **Jun Xu:** Formal analysis. **Jiazhen Wu:** Formal analysis. **Hui Chen:** Conceptualization. **Yingjie Kang:** Methodology. **Yuchan Yang:** Resources, Project administration. **Zhigang Gong:** Software, Data curation. **Yanwen Huang:** Validation. **Hui Wang:** Visualization. **Bo Wang:** Supervision, Conceptualization. **Songhua Zhan:** Writing – review & editing. **Wenli Tan:** Writing – review & editing, Conceptualization.

Declaration of competing interest

The authors declare that they have no known competing financial interests or personal relationships that could have appeared to influence the work reported in this paper.

Abbreviations

MwoA	migraine without aura
HCs	healthy controls
MVPA	multi-voxel pattern analysis
SVM	support vector machine
fMRI	functional MRI
BOLD	blood-oxygen-level dependent
FC	functional connectivity
EC	effective connectivity
ALFF	Amplitude of low-frequency fluctuation
ReHo	Regional homogeneity
VAS	visual analogue scale
SAS	Self-Rating Anxiety Scale
SDS	Self-Rating Depression Scale
MSQ	Migraine-Specific Quality of Life Questionnaire scores

MNI	Montreal Neurological Institute
fALFF	Fractional amplitude of low-frequency fluctuation
VMHC	Voxel-mirrored homotopic connectivity
DC	Degree centrality
GSC	Global signal connectivity
TDA	Temporal Dynamic Analysis
ROI	region of interest
SD	standard deviation
FWHM	full-width at half maximum
LOSOCV	leave-one-subject-out-cross-validation
MSE	mean squared error
Thalamus_R	right thalamus
Insula_L	left insula
Precentral_L	left precentral gyrus
Cuneus_R	right cuneus
Occipital_Inf_L	left inferior occipital gyrus

References

[1] G. Santangelo, A. Russo, L. Trojano, F. Falco, L. Marcuccio, M. Siciliano, F. Conte, F. Garramone, A. Tessitore, G. Tedeschi, Cognitive dysfunctions and psychological symptoms in migraine without aura: a cross-sectional study, J. Headache Pain 17 (1) (2016).

[2] M. Ashina, Z. Katsarava, T.P. Do, D.C. Buse, P. Pozo-Rosich, A. Özge, A.V. Krymchantowski, E.R. Lebedeva, K. Ravishankar, S. Yu, S. Sacco, S. Ashina, S. Younis, T.J. Steiner, R.B. Lipton, Migraine: epidemiology and systems of care, Lancet 397 (10283) (2021) 1485–1495.

[3] T.J. Schwedt, Multisensory integration in migraine, Curr. Opin. Neurol. 26 (3) (2013) 248–253.

[4] M. Leonardi, T.J. Steiner, A.T. Scher, R.B. Lipton, The global burden of migraine: measuring disability in headache disorders with WHO's Classification of Functioning, Disability and Health (ICF), J. Headache Pain 6 (6) (2005) 429–440.

[5] M. Ashina, J.M. Hansen, T.P. Do, A. Melo-Carrillo, R. Burstein, M.A. Moskowitz, Migraine and the trigeminovascular system-40 years and counting, Lancet Neurol. 18 (8) (2019) 795–804.

[6] T.J. Schwedt, C.C. Chiang, C.D. Chong, D.W. Dodick, Functional MRI of migraine, Lancet Neurol. 14 (1) (2015) 81–91.

[7] S. Schramm, C. Borner, M. Reichert, T. Baum, C. Zimmer, F. Heinen, M.V. Bonfert, N. Sollmann, Functional magnetic resonance imaging in migraine: a systematic review, Cephalalgia 43 (2) (2023) 3331024221128278.

[8] E. Szabo, A. Galambos, N. Kocsel, A.E. Edes, D. Pap, T. Zsombok, L.R. Kozak, G. Bagdy, G. Kokonyei, G. Juhasz, Association between migraine frequency and neural response to emotional faces: an fMRI study, Neuroimage Clin. 22 (2019) 101790.

[9] Y. Tu, Z. Fu, F. Zeng, N. Maleki, L. Lan, Z. Li, J. Park, G. Wilson, Y. Gao, M. Liu, V. Calhoun, F. Liang, J. Kong, Abnormal thalamocortical network dynamics in migraine, Neurology 92 (23) (2019) e2706–e2716.

[10] H.L. Wei, J. Chen, Y.C. Chen, Y.S. Yu, G.P. Zhou, L.J. Qu, X. Yin, J. Li, H. Zhang, Impaired functional connectivity of limbic system in migraine without aura, Brain Imaging Behav. 14 (5) (2020) 1805–1814.

[11] Y. Tu, F. Zeng, L. Lan, Z. Li, N. Maleki, B. Liu, J. Chen, C. Wang, J. Park, C. Lang, G. Yujie, M. Liu, Z. Fu, Z. Zhang, F. Liang, J. Kong, An fMRI-based neural marker for migraine without aura, Neurology 94 (7) (2020) e741–e751.

[12] Y. Chen, Y. Kang, S. Luo, S. Liu, B. Wang, Z. Gong, Y. Huang, H. Wang, S. Zhan, W. Tan, The cumulative therapeutic effect of acupuncture in patients with migraine without aura: evidence from dynamic alterations of intrinsic brain activity and effective connectivity, Front. Neurosci. 16 (2022).

[13] A. May, R. Burstein, Hypothalamic regulation of headache and migraine, Cephalalgia 39 (13) (2019) 1710–1719.

[14] J.V. Haxby, A.C. Connolly, J.S. Guntupalli, Decoding neural representational spaces using multivariate pattern analysis, Annu. Rev. Neurosci. 37 (2014) 435–456.

[15] K.A. Norman, S.M. Polyn, G.J. Detre, J.V. Haxby, Beyond mind-reading: multi-voxel pattern analysis of fMRI data, Trends Cognit. Sci. 10 (9) (2006) 424–430.

[16] C.W. Woo, L.J. Chang, M.A. Lindquist, T.D. Wager, Building better biomarkers: brain models in translational neuroimaging, Nat. Neurosci. 20 (3) (2017) 365–377.

[17] S. Vieira, W.H. Pinaya, A. Mechelli, Using deep learning to investigate the neuroimaging correlates of psychiatric and neurological disorders: methods and applications, Neurosci. Biobehav. Rev. 74 (Pt A) (2017) 58–75.

[18] G.H. Dong, Z. Wang, H. Dong, M. Wang, Y. Zheng, S. Ye, J. Zhang, M.N. Potenza, More stringent criteria are needed for diagnosing internet gaming disorder: evidence from regional brain features and whole-brain functional connectivity multivariate pattern analyses, J. Behav. Addict. 9 (3) (2020) 642–653.

[19] H. Li, S. Song, D. Wang, Z. Tan, Z. Lian, Y. Wang, X. Zhou, C. Pan, Individualized diagnosis of major depressive disorder via multivariate pattern analysis of thalamic sMRI features, BMC Psychiatr. 21 (1) (2021) 415.

[20] X. Zhang, L. Tao, H. Chen, X. Zhang, H. Wang, W. He, Q. Li, F. Lv, T. Luo, J. Luo, Y. Man, Z. Xiao, J. Cao, W. Fang, Combined intrinsic local functional connectivity with multivariate pattern analysis to identify depressed essential tremor, Front. Neurol. 13 (2022) 847650.

[21] C. Feng, Z. Cui, D. Cheng, R. Xu, R. Gu, Individualized prediction of dispositional worry using white matter connectivity, Psychol. Med. 49 (12) (2018) 1999–2008.

[22] Y. Han, H. Yan, X. Shan, H. Li, F. Liu, G. Xie, P. Li, W. Guo, Can the aberrant occipital-cerebellum network be a predictor of treatment in panic disorder? J. Affect. Disord. 331 (2023) 207–216.

[23] C.G. Yan, Z. Yang, S.J. Colcombe, X.N. Zuo, M.P. Milham, Concordance among indices of intrinsic brain function: insights from inter-individual variation and temporal dynamics, Sci. Bull. 62 (23) (2017) 1572–1584.

[24] Y. Tian, H.B. Chen, X.X. Ma, S.H. Li, C.M. Li, S.H. Wu, F.Z. Liu, Y. Du, K. Li, W. Su, Aberrant volume-wise and voxel-wise concordance among dynamic intrinsic brain activity indices in Parkinson's disease: a resting-state fMRI study, Front. Aging Neurosci. 14 (2022) 814893.

[25] X. Chen, O.A. Onur, N. Richter, R. Fassbender, H. Gramespacher, Q. Befahr, B. von Reutern, K. Dillen, H.I.L. Jacobs, J. Kukolja, G.R. Fink, J. Dronse, Concordance of intrinsic brain connectivity measures is disrupted in alzheimer's disease, Brain Connect. (2021).

[26] J. Zhu, Y. Zhang, B. Zhang, Y. Yang, Y. Wang, C. Zhang, W. Zhao, D.M. Zhu, Y. Yu, Abnormal coupling among spontaneous brain activity metrics and cognitive deficits in major depressive disorder, J. Affect. Disord. 252 (2019) 74–83.

[27] W. Li, C. Wang, X. Lan, L. Fu, F. Zhang, Y. Ye, H. Liu, K. Wu, Y. Zhou, Y. Ning, Variability and concordance among indices of brain activity in major depressive disorder with suicidal ideation: a temporal dynamics resting-state fMRI analysis, J. Affect. Disord. 319 (2022) 70–78.

[28] J. Zhu, D.M. Zhu, Y. Qian, X. Li, Y. Yu, Altered spatial and temporal concordance among intrinsic brain activity measures in schizophrenia, J. Psychiatr. Res. 106 (2018) 91–98.

[29] Headache classification committee of the international headache society (IHS) the international classification of headache disorders, 3rd edition, Cephalalgia 38 (1) (2018) 1–211.
[30] Y.F. Zang, Y. He, C.Z. Zhu, Q.J. Cao, M.Q. Sui, M. Liang, L.X. Tian, T.Z. Jiang, Y.F. Wang, Altered baseline brain activity in children with ADHD revealed by resting-state functional MRI, Brain Dev. 29 (2) (2007) 83–91.
[31] Q.H. Zou, C.Z. Zhu, Y. Yang, X.N. Zuo, X.Y. Long, Q.J. Cao, Y.F. Wang, Y.F. Zang, An improved approach to detection of amplitude of low-frequency fluctuation (ALFF) for resting-state fMRI: fractional ALFF, J. Neurosci. Methods 172 (1) (2008) 137–141.
[32] C.G. Yan, R.C. Craddock, X.N. Zuo, Y.F. Zang, M.P. Milham, Standardizing the intrinsic brain: towards robust measurement of inter-individual variation in 1000 functional connectomes, Neuroimage 80 (2013) 246–262.
[33] Y. Zang, T. Jiang, Y. Lu, Y. He, L. Tian, Regional homogeneity approach to fMRI data analysis, Neuroimage 22 (1) (2004) 394–400.
[34] X.N. Zuo, C. Kelly, A. Di Martino, M. Mennes, D.S. Margulies, S. Bangaru, R. Grzadzinski, A.C. Evans, Y.F. Zang, F.X. Castellanos, M.P. Milham, Growing together and growing apart: regional and sex differences in the lifespan developmental trajectories of functional homotopy, J. Neurosci. 30 (45) (2010) 15034–15043.
[35] X.N. Zuo, R. Ehmke, M. Mennes, D. Imperati, F.X. Castellanos, O. Sporns, M.P. Milham, Network centrality in the human functional connectome, Cerebr. Cortex 22 (8) (2012) 1862–1875.
[36] A. Hahamy, V. Calhoun, G. Pearlson, M. Harel, N. Stern, F. Attar, R. Malach, R. Salomon, Save the global: global signal connectivity as a tool for studying clinical populations with functional magnetic resonance imaging, Brain Connect. 4 (6) (2014) 395–403.
[37] C.G. Yan, X.D. Wang, X.N. Zuo, Y.F. Zang, DPABI: data processing & analysis for (Resting-State) brain imaging, Neuroinformatics 14 (3) (2016) 339–351.
[38] F. Lou, J. Tao, R. Zhou, S. Chen, A. Qian, C. Yang, X. Zheng, B. Chen, Z. Hu, M. Wang, Altered variability and concordance of dynamic resting-state fMRI indices in patients with attention deficit hyperactivity disorder, Front. Neurosci. 15 (2021) 731596.
[39] J. Schrouff, M.J. Rosa, J.M. Rondina, A.F. Marquand, C. Chu, J. Ashburner, C. Phillips, J. Richiardi, J. Mourão-Miranda, PRoNTo: pattern recognition for neuroimaging Toolbox, Neuroinformatics 11 (3) (2013) 319–337.
[40] Q. Gong, L. Li, S. Tognin, Q. Wu, W. Pettersson-Yeo, S. Lui, X. Huang, A.F. Marquand, A. Mechelli, Using structural neuroanatomy to identify trauma survivors with and without post-traumatic stress disorder at the individual level, Psychol. Med. 44 (1) (2014) 195–203.
[41] Z. Wang, H. Dong, X. Du, J.T. Zhang, G.H. Dong, Decreased effective connection from the parahippocampal gyrus to the prefrontal cortex in Internet gaming disorder: a MVPA and spDCM study, J. Behav. Addict. 9 (1) (2020) 105–115.
[42] M. Cai, J. Liu, X. Wang, J. Ma, L. Ma, M. Liu, Y. Zhao, H. Wang, D. Fu, W. Wang, Q. Xu, L. Guo, F. Liu, Spontaneous brain activity abnormalities in migraine: a meta-analysis of functional neuroimaging, Hum. Brain Mapp. 44 (2) (2023) 571–584.
[43] H.L. Wei, T. Tian, G.P. Zhou, J.J. Wang, X. Guo, Y.C. Chen, Y.S. Yu, X. Yin, J. Li, H. Zhang, Disrupted dynamic functional connectivity of the visual network in episodic patients with migraine without aura, Neural Plast. 2022 (2022) 9941832.
[44] L. Michels, J. Villanueva, R. O'Gorman, M. Muthuraman, N. Koirala, R. Buchler, A.R. Gantenbein, P.S. Sandor, R. Luechinger, S. Kollias, F. Riederer, Interictal hyperperfusion in the higher visual cortex in patients with episodic migraine, Headache 59 (10) (2019) 1808–1820.
[45] L. Zhao, J. Liu, X. Yan, W. Dun, J. Yang, L. Huang, Y. Kai, D. Yu, W. Qin, T. Jie, F. Liang, Abnormal brain activity changes in patients with migraine: a short-term longitudinal study, J. Clin. Neurol. 10 (3) (2014) 229–235.
[46] J.J. Wang, X. Chen, S.K. Sah, C. Zeng, Y.M. Li, N. Li, M.Q. Liu, S.L. Du, Amplitude of low-frequency fluctuation (ALFF) and fractional ALFF in migraine patients: a resting-state functional MRI study, Clin. Radiol. 71 (6) (2016) 558–564.
[47] S. Liu, S. Luo, T. Yan, W. Ma, X. Wei, Y. Chen, S. Zhan, B. Wang, Differential modulating effect of acupuncture in patients with migraine without aura: a resting functional magnetic resonance study, Front. Neurol. 12 (2021) 680896.
[48] D. Zhang, X. Huang, C. Mao, Y. Chen, Z. Miao, C. Liu, C. Xu, X. Wu, X. Yin, Assessment of normalized cerebral blood flow and its connectivity with migraines without aura during interictal periods by arterial spin labeling, J. Headache Pain 22 (1) (2021) 72.
[49] M. Lisicki, K. D'Ostilio, G. Coppola, V. Parisi, A.M. de Noordhout, D. Magis, J. Schoenen, F. Scholtes, J. Versijpt, Age related metabolic modifications in the migraine brain, Cephalalgia 39 (8) (2019) 978–987.
[50] R. Noseda, R. Burstein, Migraine pathophysiology: anatomy of the trigeminovascular pathway and associated neurological symptoms, cortical spreading depression, sensitization, and modulation of pain, Pain 154 (Supplement 1) (2013) S44–S53.
[51] G. Chen, Y. Li, Z. Dong, R. Wang, D. Zhao, I. Obeso, S. Yu, Response inhibition alterations in migraine: evidence from event-related potentials and evoked oscillations, J. Headache Pain 21 (1) (2020) 119.
[52] J. Hoffmann, S. Miller, M. Martins-Oliveira, S. Akerman, W. Supronsinchai, H. Sun, L. Shi, J. Wang, D. Zhu, S. Lehto, H. Liu, R. Yin, B.D. Moyer, C. Xu, P. J. Goadsby, PAC1 receptor blockade reduces central nociceptive activity: new approach for primary headache? Pain 161 (7) (2020) 1670–1681.
[53] A. Russo, V. Marcelli, F. Esposito, V. Corvino, L. Marcuccio, A. Giannone, R. Conforti, E. Marciano, G. Tedeschi, A. Tessitore, Abnormal thalamic function in patients with vestibular migraine, Neurology 82 (23) (2014) 2120–2126.
[54] M. Lim, H. Jassar, D.J. Kim, T.D. Nascimento, A.F. DaSilva, Differential alteration of fMRI signal variability in the ascending trigeminal somatosensory and pain modulatory pathways in migraine, J. Headache Pain 22 (1) (2021) 4.
[55] A. Russo, A. Tessitore, M. Silvestro, F. Di Nardo, F. Trojsi, T. Del Santo, R. De Micco, F. Esposito, G. Tedeschi, Advanced visual network and cerebellar hyperresponsiveness to trigeminal nociception in migraine with aura, J. Headache Pain 20 (1) (2019) 46.
[56] Z. Chen, R. Zhang, H. Huo, P. Liu, C. Zhang, T. Feng, Functional connectome of human cerebellum, Neuroimage 251 (2022) 119015.
[57] A. Riou, J.F. Houvenaghel, T. Dondaine, S. Drapier, P. Sauleau, D. Drapier, J. Duprez, M. Guillery, F. Le Jeune, M. Verin, G. Robert, Functional role of the cerebellum in Parkinson disease: a PET study, Neurology 96 (23) (2021) e2874–e2884.
[58] B.T. Craig, A. Morrill, B. Anderson, J. Danckert, C.L. Striemer, Cerebellar lesions disrupt spatial and temporal visual attention, Cortex 139 (2021) 27–42.
[59] J. Mu, T. Chen, S. Quan, C. Wang, L. Zhao, J. Liu, Neuroimaging features of whole-brain functional connectivity predict attack frequency of migraine, Hum. Brain Mapp. 41 (4) (2020) 984–993.
[60] S. Ye, M. Wang, Q. Yang, H. Dong, G.H. Dong, Predicting the severity of internet gaming disorder with resting-state brain features: a multi-voxel pattern analysis, J. Affect. Disord. 318 (2022) 113–122.
[61] S. Harricharan, A.A. Nicholson, J. Thome, M. Densmore, M.C. McKinnon, J. Theberge, P.A. Frewen, R.W.J. Neufeld, R.A. Lanius, PTSD and its dissociative subtype through the lens of the insula: anterior and posterior insula resting-state functional connectivity and its predictive validity using machine learning, Psychophysiology 57 (1) (2020) e13472.